

Thermally driven spin injection from a ferromagnet into a non-magnetic metal

A. Slachter,* F. L. Bakker, J. -P. Adam, and B. J. van Wees

Physics of Nanodevices, Zernike Institute for Advanced Materials, University of Groningen, The Netherlands

(Dated: October 29, 2018)

Creating, manipulating and detecting spin polarized carriers are the key elements of spin based electronics^{1,2}. Most practical devices³⁻⁵ use a perpendicular geometry in which the spin currents, describing the transport of spin angular momentum, are accompanied by charge currents. In recent years, new sources of pure spin currents, i.e., without charge currents, have been demonstrated⁶⁻⁹ and applied¹⁰⁻¹³. In this paper, we demonstrate a conceptually new source of pure spin current driven by the flow of heat across a ferromagnetic/non-magnetic metal (FM/NM) interface. This spin current is generated because the Seebeck coefficient, which describes the generation of a voltage as a result of a temperature gradient, is spin dependent in a ferromagnet^{14,15}. For a detailed study of this new source of spins, it is measured in a non-local lateral geometry. We developed a 3D model that describes the heat, charge and spin transport in this geometry which allows us to quantify this process⁵. We obtain a spin Seebeck coefficient for Permalloy of -3.8 $\mu\text{V}/\text{K}$ demonstrating that thermally driven spin injection is a feasible alternative for electrical spin injection in, for example, spin transfer torque experiments¹⁷.

The interplay of spin dependent conductivity and thermoelectricity was already known for half a century where it was used to describe the conventional Seebeck effect of ferromagnetic metals³. The discovery of the GMR effect³ sparked the interest of the community in spin dependent conductivity and novel spin electronics which is going on until today^{4,5,8,19}. Due to experimental difficulties in controlling heat flows it was only until very recent that thermoelectric spintronics was investigated²⁰⁻²² leading to the new field of spin caloritronics¹⁴. A relevant example is given by Uchida *et al.*⁹ who interpreted their results in terms of the generation of a *bulk* spin accumulation due to an applied temperature gradient in a ferromagnet film. In contrast, the effect we describe in this paper arises from a heat current flowing through a ferromagnetic/non magnetic metal junction (FM/NM) which creates a spin accumulation at the *interface*.

The concept of how we generate a heat current over a FM/NM junction and subsequently measure the spin accumulation is shown in figure 1. The scheme is essentially a lateral non local spin valve structure⁶ with the electrical injection replaced by thermal spin injection. We use this non local scheme to separate spin injection from possible spurious effects^{6,12,13} and because the observed thermally generated non-spin related voltage, which we

refer to as the baseline resistance, allows to extract the temperature distribution in the device by comparing this to modeling⁵.

We first formulate an appropriate diffusive transport theory for thermally driven spin injection. The Seebeck coefficient describes that an applied temperature gradient across a conductor generates an electric field²⁵. In a ferromagnet, the transport processes for the majority and minority spin are different leading to a spin dependent conductivity $\sigma_{\uparrow,\downarrow}$ and Seebeck coefficient $S_{\uparrow,\downarrow}$ ^{3,15}. The first is used to describe magnetoelectronics²⁶ in FM/NM systems where the latter one is usually disregarded. In order to consider what happens when heat is sent through the system, we write the spin dependent currents:

$$J_{\uparrow,\downarrow} = -\sigma_{\uparrow,\downarrow} \left(\frac{1}{e} \nabla \mu_{\uparrow,\downarrow} - S_{\uparrow,\downarrow} \nabla T \right) \quad (1)$$

here $\mu_{\uparrow,\downarrow}$ is the spin dependent chemical potential. When a heat current Q is sent through a ferromagnet in the absence of a charge current, a spin current $J_s = J_{\uparrow} - J_{\downarrow} =$

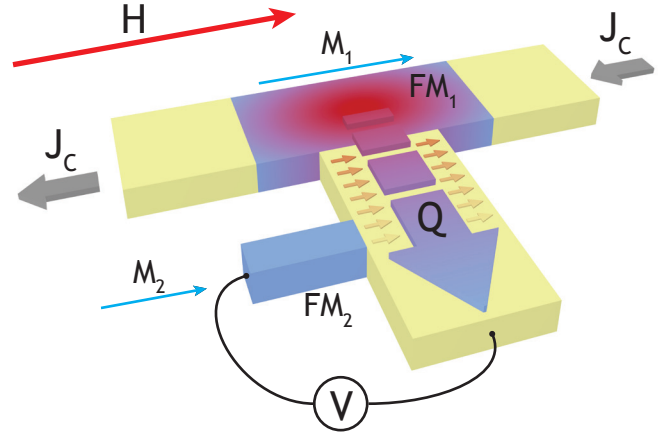


FIG. 1: **Conceptual diagram.** A charge current J_C is sent through ferromagnet 1 (FM₁) causing Joule heating due to the large resistivity of FM₁. The NM contacts (yellow) are highly thermally conductive, thereby providing heat sinks. The heat current Q through the center FM₁/NM interface injects a spin current into the NM depending on the magnetization direction M_1 . The generated spins diffuse towards the FM₂/NM interface where they generate a potential $\Delta\mu = P\mu_s$ depending on the magnetization direction M_2 . As a consequence of Joule heating, the signal expected to arise from thermal spin injection scales with $\nabla T \propto I^2$. This potential is measured using the indicated voltage scheme by selectively switching the magnetization directions M_1 and M_2 by a magnetic field H .

$\sigma_F(1 - P^2)S_s\nabla T/2$ flows driven by the spin Seebeck coefficient $S_s = S_\uparrow - S_\downarrow$. Here P is the current polarization of the ferromagnet and σ_F is the conductivity of the ferromagnet.

To quantify the thermal injection of spins we consider the FM/NM interface and solve the Valet-Fert equation² in a fashion similar as van Son et al¹ (Supplementary Information A). The result is depicted in figure 2. A spin accumulation appears at the interface driven by the abrupt change of spin current going from the bulk FM to the bulk NM, thereby acting as an effective source of spins at the interface. The resulting spin accumulation has the following expression:

$$\frac{\mu_s}{\nabla T_{FM}} = e\lambda_F S_s R_{mis} \quad (2)$$

where $R_{mis} = R_N/(R_N + R_F/(1 - P^2))$ is a conductivity mismatch⁴ factor in which $R_i = \lambda_i/\sigma_i$ are the spin resistances determined by the relaxation lengths λ_i and the conductivities σ_i . For the metallic interfaces under consideration in this paper, this factor is very close to 1. The resulting spin accumulation induced by the heat flow $Q = -k_{FM}\nabla T_{FM}$ is determined solely by the spin Seebeck coefficient S_s and the ferromagnetic spin relaxation length λ_F . Its direction is determined by the sign

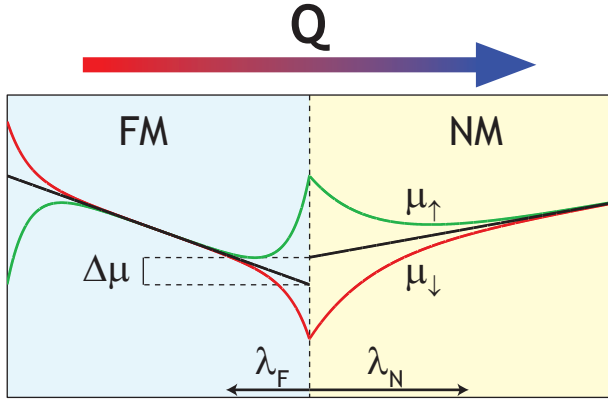


FIG. 2: **Thermal spin injection by the spin Seebeck coefficient across a FM/NM interface.** Schematic figure showing the resulting spin dependent chemical potentials $\mu_{\uparrow,\downarrow}$ across a FM/NM interface when a heat current $Q = -k\nabla T$ crosses it. Heat current is taken to be continuous across the interface leading to a discontinuity in ∇T . No currents are allowed to leave the FM, nevertheless, a spin current proportional to the spin Seebeck coefficient flows through the bulk FM which needs to become unpolarized in the bulk NM. This creates a spin imbalance $\mu_\uparrow - \mu_\downarrow$ at the boundary which relaxes in the FM and NM on the length scale of their respective spin relaxation lengths λ_i . A thermoelectric interface potential $\Delta\mu = P\mu_s$ also builds up. On the left side no spin current is allowed to leave leading to a spin accumulation of opposite sign.

of the spin Seebeck coefficient which changes sign when the magnetization of the ferromagnet reverses.

Using a lock-in technique we determine the relevant parameters $R_1(\mu V/mA)$ and $R_2(\mu V/mA^2)$ from the observed voltage⁵:

$$V = R_1 I + R_2 I^2 + \dots \quad (3)$$

The baseline resistance, defined in terms of a parallel and antiparallel contribution as $(R_i^P + R_i^{AP})/2 = R_i^b$, allows to extract the magnitude of Joule and Peltier heating effects and possible conventional Ohmic potential drops⁵. Here R_1^b is determined by the Ohmic potential drop and Peltier heating/cooling measured by the FM₂-NM thermocouple while the baseline resistance R_2^b is determined by Joule heating measured by the same thermocouple. The spin dependent contribution $R_i^P - R_i^{AP} = R_i^s$ to R_1 is due to a conventional spin valve signal while this contribution to R_2 comes from thermal spin injection.

A dedicated device was fabricated to study this effect and is shown in figure 3. The heating of FM₁ has been kept very localized to an area of $150 \times 150 \text{ nm}^2$ by using thick gold contacts. Moreover, the contacts are placed asymmetrically to minimize the possible current flowing in and out of the FM₁/NM interface. An additional contact 5 is present to be able to send a current directly through the FM₁/NM interface. By comparing the obtained signal R_1^s to a model (see methods), we can extract the spin injection/detection efficiency⁵, which has been made as high as possible by keeping the size of

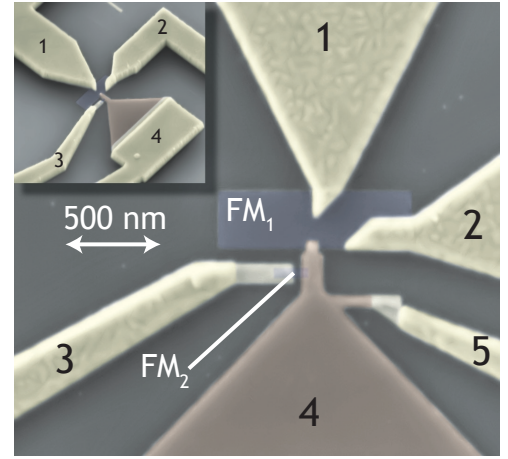


FIG. 3: **Coloured SEM picture of the fabricated device.** The device consists of two 15 nm thick Permalloy ($\text{Ni}_{80}\text{Fe}_{20}$) ferromagnets FM₁ and FM₂ of $1 \mu\text{m} \times 300 \text{ nm}$ and $150 \times 40 \text{ nm}^2$ separated from each other by 100 nm. They are connected by a 60 nm thick copper funnel with small effective FM/NM contact areas of $40 \times 40 \text{ nm}^2$ and $30 \times 40 \text{ nm}^2$. 5/175 nm thick Ti/Au contacts 1 and 2 are placed asymmetrically on FM₁ to Joule heat it while contacts 3 and 4 are used to measure Joule heating and thermal spin injection. An additional contact 5 is present to measure a regular non-local spin valve signal.

the FM/NM contacts small. All measurements are performed at room temperature.

Figure 4 shows our principal results on thermal spin injection. Four distinct P-AP and AP-P switches are observed up to 70 nV in magnitude scaling with I^2 on a large background originating from the Py_2/Cu thermocouple.

The interpretation of the obtained signals requires a detailed knowledge of the heat, charge and spin currents in the device. For this purpose a 3D thermoelectric spin model was constructed which extends the spin-dependent current model² to include thermoelectricity as well as thermal spin injection by the spin Seebeck coefficient.

The calculated average contribution R_2^b is $2.4 \mu\text{V}/\text{mA}^2$ slightly lower than the observed $7.69 \mu\text{V}/\text{mA}^2$. The difference between the observed and modelled value was seen before in non-local spin valve samples⁵. It can be explained by a reduction in the Permalloy thickness due to its oxidation, which effectively increases the Joule heating. In the following, we scale the overall Joule heating in our model to fit our measured result R_2^b . We then find that we were able to heat FM_1 to a maximum of $\approx 40\text{K}$ at which ∇T_{FM} at the FM_1/NM interface is $\approx 50 \text{K}/\mu\text{m}$. At this moment the current density is $\approx 8 \times 10^{11} \text{A}/\text{m}^2$, close to the point where the device will fail due to electromigration.

Electrical spin injection was also measured and the results are shown in figure 5c. A relatively large 9 m Ω spin valve signal is present on top of a 1.05 Ω background, being only slightly different to the 7.8 m Ω and 640 m Ω

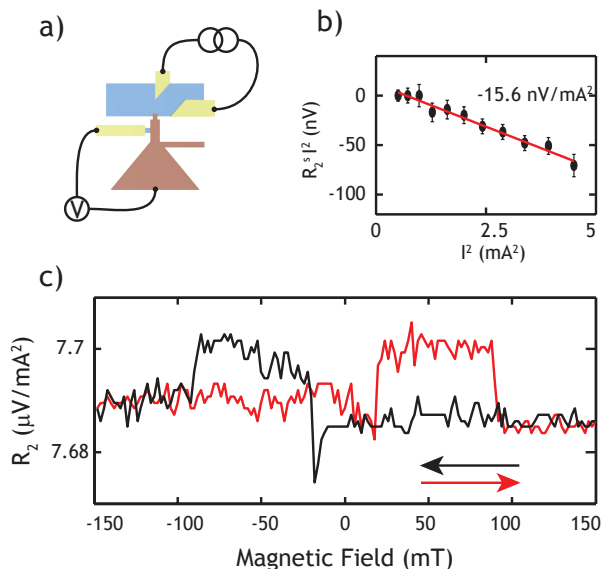


FIG. 4: **Thermal spin injection measurements.** **a**, Measurement scheme of the experiment. **b**, Second harmonic measurement result $R_2^b I^2$ (nV) of the observed thermal spin signal as a function of I^2 . **c**, Measured second harmonic signal at a rms current of 1.5 mA showing the four distinct switches resulting from the magnetization alignment of FM_1 and FM_2 illustrating thermal spin injection.

calculated signals with the metallic spin parameters $\lambda_{\text{Cu}} = 350 \text{nm}$, $\lambda_{\text{Py}} = 5 \text{nm}$ and $P_{\text{Py}} = 0.25$ obtained from previously fabricated samples^{5,6}. Here P_{Py} is positive as shown before²⁸.

The observed thermal spin injection signal $R_2^s = -15.6 \text{nV}/\text{mA}^2$ is determined from figure 4b. We obtain a spin Seebeck coefficient for Permalloy of $-3.8 \mu\text{V}/\text{K}$, a fraction of the conventional Seebeck coefficient $S_F = -20 \mu\text{V}/\text{K}$ ⁹. This gives a polarization of the Seebeck coefficient of $P_S = S_s/S_F = 0.19$ not too different from the spin polarization of the current. It is significantly larger than the $S_s = -2 \text{nV}/\text{K}$ coefficient extracted by Uchida et al.⁹. However, it is in good agreement with recent theoretical predictions^{15,17}.

In addition to the thermal spin injection signal, a small regular spin valve signal $R_1^s = -20 \mu\Omega$ is also present and is shown in figure 5a. The baseline resistance R_1^b of 90 $\mu\Omega$ is in line with the calculated 95 $\mu\Omega$. This is caused by Peltier heating and cooling of the two current injecting contacts⁵.

The negative regular spin valve signal R_1^s can be un-

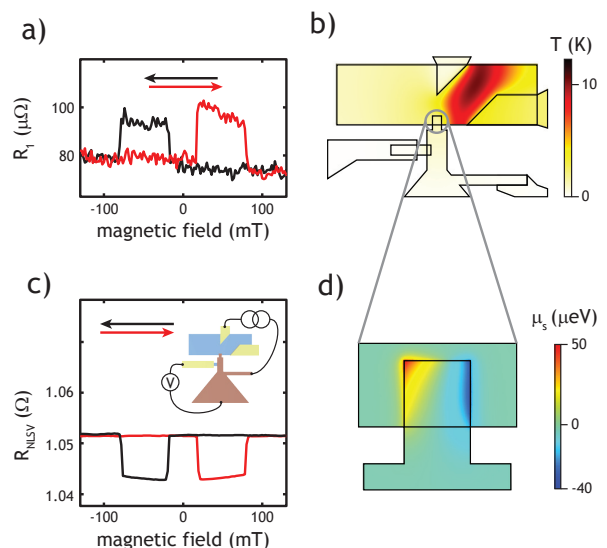


FIG. 5: **Rectification effects and electrical spin injection.** **a**, first harmonic measurement R_1 for the measurement setup of figure 4. **b**, Calculated temperature distribution at a height of 10 nm with a current of 2 mA sent through FM_1 . It illustrates the localized Joule heating, Peltier cooling and heating of the two Au/Py current injecting contacts and subsequent thermal conduction towards the three connected metallic contacts. **c**, Measured electrical spin injection scheme and resulting spin valve. **d**, Calculated spin accumulation at a height of 10 nm. A small part of the current path is short circuited by the Cu connection so that 4% still flows in and out of the Py_1/Cu contact because of its large conductivity. This creates a large positive and negative spin accumulation. Due to the asymmetry in spin injection and the asymmetrical placement at FM_2 a small fraction of 3% is still predicted to give a small regular spin valve signal R_1^S .

derstood as follows. Due to the high conductivity of the copper, a fraction of the current flows into and out of Cu/Py₁ interface electrically injecting spins. A small net spin accumulation at the detector interface remains caused by the asymmetric placement of FM₂. It is illustrated by the calculation of the spin accumulation at the Py₁/Cu interface shown in figure 5d which shows the high geometrical dependence of this effect. The observed R_1^s is somewhat smaller than the calculated $-45 \mu\Omega$. We believe that the small $40 \times 40 \text{ nm}^2$ size of the copper contact makes sure copper grain size, lithographic precision and ballistic effects start dominating the magnitude of this effect.

A previous device showed a thermal spin injection signal -5 nV/mA^2 at a FM-FM distance of 400 nm, only visible at the highest current (Supplementary information B). A similar calculation gives $S_s^{Py} = -5 \mu\text{V/K}$ in agreement with the analysis for the sample presented.

Now that the parameters governing equation 2 are known we may compare this to the electrical spin injection results for the transparent Cu/Py interface. We can calculate that for thermal spin injection $\mu_S/\nabla T \approx 2 \times 10^{-14} \text{ eV m/K}$ versus $\mu_S/J \approx 3 \cdot 10^{-16} \text{ eV m}^2/\text{A}$ for electrical spin injection through a transparent Cu/Py

contact.

Due to the lateral non-local geometry and Joule heating method used in this paper, we are limited to a maximum temperature gradient of $\approx 50 \text{ K}/\mu\text{m}$. However, in a typical perpendicular geometry switching by spin transfer torque⁵ this does not have to be the case. In order to switch the magnetization by electrical spin transfer torque one needs a typical charge current density of $\approx 5 \cdot 10^{11} \text{ A/m}^2$. The same stack should be able to switch by applying a temperature difference of only a few tens of degrees as earlier theoretical studies have indicated^{15,17}. This simple example shows that despite the weak signals observed in this paper, this process can be a very viable alternative, or even work alongside, electrical spin injection.

In conclusion we have demonstrated the concept of thermal spin injection in a lateral metallic Py/Cu system. By constructing a theory for thermal spin injection and comparing the observed potential to detailed 3D modeling, we were able to extract a spin Seebeck coefficient for Permalloy of $-3.8 \mu\text{V/K}$. This demonstrates thermal spin injection is a feasible alternative for electrical spin injection in for example spin transfer torque experiments¹⁷.

* Electronic address: A.Slachter@rug.nl

¹ Zutic, I., Fabian, J. & Das Sarma, S. Spintronics: fundamentals and applications. *Rev. Mod. Phys.* **76**, 323-410 (2004)

² Chappert, C., Fert, A. & Nguyen van Dau, F. The emergence of spin electronics in data storage. *Nature Mater.* **6**, 813-823 (2007)

³ Baibich, M.N. *et al.* Giant magnetoresistance of (001)Fe/(001)Cr magnetic superlattices. (*Phys. Rev. Lett.*) **61**, 2472-2475 (1988)

⁴ Kiselev, S.I. *et al.* Microwave oscillations of a nanomagnet driven by a spin-polarized current. *Nature* **425**, 380-383 (2003)

⁵ Albert, F.J., Katine, J.A., Buhrman, R.A. & Ralph, D.C. Spin-polarized current switching of a Co thin film nanomagnet. *Appl. Phys. Lett.* **77**, 3809-3811 (2000)

⁶ Jedema, F.J., Filip, A. & van Wees, B.J. Electrical spin injection and accumulation at room temperature in an all-metal mesoscopic spin valve. *Nature* **410**, 345-348 (2001)

⁷ Valenzuela, S.O. & Tinkham, M. Direct electronic measurement of the spin Hall effect. *Nature* **442**, 176-179 (2006)

⁸ Costache, M.V., Sladkov, M., Watts, S.M., van der Wal, C.H. & van Wees, B.J. Electrical Detection of Spin Pumping due to the Precessing Magnetization of a Single Ferromagnet. *Phys. Rev. Lett.* **97**, 216603 (2006)

⁹ Uchida, K. *et al.* Observation of the Spin Seebeck effect. *Nature* **455**, 778-781 (2008)

¹⁰ Yang, T., Kimura, T. & Otani, Y. Giant spin-accumulation signal and pure spin-current-induced reversible magnetization switching. *Nature Phys.* **4**, 851-854 (2008)

¹¹ Kimura, T., Otani, Y., Sato, T., Takahashi, S. & Maekawa, S. Room-Temperature Reversible Spin Hall Effect. *Phys. Rev. Lett.* **98**, 156601 (2007)

¹² Lou, X. *et al.* Electrical detection of spin transport in lateral ferromagnetsemiconductor devices. *Nature Phys.* **3**, 197-202 (2007)

¹³ Dash, S.P., Sharma, S., Patel, R.S., de Jong, M.P. & Jansen, R. Electrical creation of spin polarization in silicon at room temperature. *Nature* **462**, 491-494 (2009)

¹⁴ Bauer, G.E., MacDonald, A.H. & Maekawa, S. Spin Caloritronics. *Solid State Commun.* **150**, 459 (2010)

¹⁵ Tulapurkar, A.A., Suzuki, Y. Contribution of electron-magnon scattering to the spin-dependent Seebeck effect in a ferromagnet. *Solid State Commun.* **150**, 466-470 (2010)

¹⁶ Bakker, F.I., Slachter, A., Adam, J.-P. & van Wees, B.J. Interplay of Peltier and Seebeck effects in nanoscale nonlocal spin valves, arXiv:1004.0118v1 (submitted to *Phys. Rev. Lett.*)

¹⁷ Hatami, M., Bauer, G.E.W., Zhang, Q. & Kelly, P.J. Thermal Spin-Transfer Torque in Magnetoelectronic Devices. *Phys. Rev. Lett.* **99**, 066603 (2007)

¹⁸ Barnard R.D. Thermoelectricity in metals and alloys. (Taylor and Francis LTD., London, 1972)

¹⁹ Tserkovnyak, Y., Brataas, A., Bauer, G.E.W. & Halperin, B.I. Nonlocal magnetization dynamics in ferromagnetic heterostructures. *Rev. Mod. Phys.* **77**, 1375-1421 (2005)

²⁰ Gravier, L., Serrano-Guisan, S., Reuse, F. & Ansermet, J.P. Thermodynamic description of heat and spin transport in magnetic nanostructures. *Phys. Rev. B* **73**, 024419 (2006)

²¹ Gravier, L., Serrano-Guisan, S., Reuse, F. & Ansermet, J.P. Spin-dependent Peltier effect of perpendicular currents in multilayered nanowires. *Phys. Rev. B* **73**, 052410 (2006)

²² Dubi, Y. & Di Ventra, M. Thermospin effects in a quantum dot connected to ferromagnetic leads. *Phys. Rev. B* **79**, 081302 (2009)

²³ Valet, T. & Fert, A. Theory of the perpendicular mag-

netoresistance in magnetic multilayers. *Phys. Rev. B*. **48**, 7099-7113 (1993)

- ²⁴ van Son, P.C., van Kempen, H. & Wyder, P. Boundary Resistance of the Ferromagnetic-Nonferromagnetic Metal Interface. *Phys. Rev. Lett.* **58**, 2271-2273 (1987)
- ²⁵ Mott, N.F. and Jones, H. *The Theory of the Properties of Metals and Alloys* (Oxford Univ. Press, London, 1936)
- ²⁶ Brataas, A., Bauer, G.E.W. & Kelly, P.J. Non-collinear magnetoelectronics. *Phys. Rep.* **427**, 157-255 (2006)
- ²⁷ Schmidt, G., Ferrand, D., Molenkamp, L.W., Filip, A.T. & van Wees, B.J. Fundamental obstacle for electrical spin injection from a ferromagnetic metal into a diffusive semiconductor. *Phys. Rev. B* **62**, R4790 (2000)
- ²⁸ Vlaminck, V., Bailleul, M. Current-Induced Spin-Wave Doppler Shift. *Science* **322**, 410 (2008)
- ²⁹ Kittel, C. *Introduction to Solid State Physics* (John Wiley & Sons, Inc., New York, 1996)

I. ACKNOWLEDGEMENTS

We would like to acknowledge J.G. Holstein, B. Wolfs and S. Bakker for technical assistance and T. Banarjee, P. Zomer and S. Denega for reading the manuscript. This work was financed by the European EC Contracts No. IST-033749 "DynaMax", the "Stichting voor Fundamenteel Onderzoek der Materie" (FOM) and NanoNed.

II. METHODS

A. Fabrication

The sample in this paper was fabricated by a 1 step optical and 5 step electron beam lithography process. In each step, metals are deposited using e-beam deposition. For the e-beam lithography process a PMMA 950K resist is used of 70-400 nm thickness depending on the thickness of the deposited material and resilience to Ar ion milling. The first e-beam lithography process produces 5/30 nm thick and 100 nm wide Ti/Au markers which using an automatic alignment procedure can be aligned to in the next e-beam deposition steps with high precision. In the next four steps, the 15 nm Py, 5/30 nm Ti/Au, 5/180 nm Ti/Au and 65 nm Cu layers are deposited. For the last three steps, Ar ion milling was used prior to deposition to remove any polymer residue and the Py oxide to obtain our highly ohmic contacts.

B. Measurements

The measurements were performed using a AC current source of a frequency $< 1\text{kHz}$ far below the characteristic thermoelectric time scale of such sized systems of $\approx 1\text{-}100\text{ ns}$. The obtained signal is sent to 3 Lock-in systems measuring the 1st, 2nd and 3rd harmonic response simultaneously. Care was taken in deriving R_1 , R_2 and

R_3 by scanning the current to make sure that even higher harmonics were negligible.

C. Modeling

We constructed a 3D model of the fabricated sample using the finite element program Comsol Multiphysics. The physics is defined in terms of a thermoelectric spin model where the spin up, down and heat currents are given by:

$$\begin{pmatrix} \vec{J}_\uparrow \\ \vec{J}_\downarrow \\ \vec{Q} \end{pmatrix} = - \begin{pmatrix} \sigma_\uparrow & 0 & -\sigma_\uparrow S_\uparrow \\ 0 & \sigma_\downarrow & -\sigma_\downarrow S_\downarrow \\ -\sigma_\uparrow \Pi_\uparrow & -\sigma_\downarrow \Pi_\downarrow & k \end{pmatrix} \cdot \begin{pmatrix} \vec{\nabla} \mu_\uparrow / e \\ \vec{\nabla} \mu_\downarrow / e \\ \vec{\nabla} T \end{pmatrix} \quad (4)$$

where $\Pi_{\uparrow,\downarrow}$ are the spin dependent Peltier coefficients given by $S_{\uparrow,\downarrow} \cdot T_0$. Here $T_0 = 300\text{K}$ which is the reference temperature of the device. We take these currents to be continuous across boundaries. At the end of all contacts we set the temperature to be T_0 . At contact 1 in figure 3 we set $J_{\uparrow,\downarrow} = J/2$ to inject a charge current which is being sent through the system by setting $\mu_{\uparrow,\downarrow} = 0$ at contact 2 or 5. At all other interfaces the currents are set to 0. We include Valet-Fert spin relaxation by assuming $\nabla J_{\uparrow,\downarrow} = \pm \frac{(1-P^2)\sigma_i}{4\lambda_i^2} (\mu_\uparrow - \mu_\downarrow)$ in the bulk. Joule heating is included

by assuming $\nabla Q = \zeta \left(\frac{\vec{J}_\uparrow^2}{\sigma_\uparrow} + \frac{\vec{J}_\downarrow^2}{\sigma_\downarrow} \right)$ where a scaling factor $\zeta = 3.2$ is used to make the model correspond to the measured R_2^b . The system was meshed most accurately at the FM/NM interfaces where the mesh size was 1 nm in order to accurately calculate thermal spin injection. The dependencies $R_1^{(s)}$ up till $R_4^{(s)}$ were determined by calculating the results at ± 1 & 2 mA for the parallel and antiparallel configuration. The measured resistivities $\sigma_{Au} = 2.2 \cdot 10^7\text{ S/m}$, $\sigma_{Cu} = 4.26 \cdot 10^7\text{ S/m}$ and $\sigma_{Py} = 4.32 \cdot 10^6\text{ S/m}$ were taken as inputs for the model. In this model, the substrate was also taken into account⁵. The Seebeck coefficients $S_{Au} = 1.7\text{ }\mu\text{V/K}$, $S_{Cu} = 1.6\text{ }\mu\text{V/K}$, $S_{Py} = -20\text{ }\mu\text{V/K}$ and thermal conductances $k_{Au} = 300\text{ W/m/K}$, $k_{Cu} = 300\text{ W/m/K}$, $k_{Py} = 30\text{ W/m/K}$, $k_{substrate} = 1\text{ W/m/K}$ were taken from various sources in literature^{9,29}.

III. SUPPLEMENTARY INFORMATION A

Here we calculate in more detail what happens when heat is sent through the FM/NM system in figure 6. We begin by writing the spin dependent currents:

$$J_{\uparrow,\downarrow} = -\sigma_{\uparrow,\downarrow} \left(\frac{1}{e} \nabla \mu_{\uparrow,\downarrow} - S_{\uparrow,\downarrow} \nabla T \right) \quad (5)$$

here $\mu_{\uparrow,\downarrow}$ is the spin dependent chemical potential. When a heat current Q is sent through a bulk ferromagnet in the absence of a charge current, a spin current $J_s =$

$J_{\uparrow} - J_{\downarrow} = \sigma_F(1 - P^2)S_s\nabla T/2$ flows, driven by the spin Seebeck coefficient $S_s = S_{\uparrow} - S_{\downarrow}$. Here P is the current polarization of the FM and σ_F is the conductivity of the ferromagnet. Charge and spin current conservation^{1,2} leads to the thermoelectric spin diffusion equation:

$$\nabla^2\mu_s = \frac{\mu_s}{\lambda^2} + e\left(\frac{dS_s}{dT}(\nabla T)^2 + S_s\nabla^2 T\right) \quad (6)$$

where μ_s is the spin accumulation $\mu_{\uparrow} - \mu_{\downarrow}$. In addition to the Valet-Fert spin diffusion equation $\nabla^2\mu_s = \frac{\mu_s}{\lambda^2}$ two source terms are present. Both terms can create (albeit small) bulk spin accumulations.

In figure 6 we send a heat current Q through the FM/NM interface while we allow no charge or spin current to leave. The heat current $Q = -k\nabla T$ needs to be continuous throughout the system, leading to $\nabla T_{FM} = k_{NM}/k_{FM}\nabla T_{NM}$ at the interface. Since ∇T is constant in both regions individually, and for first order effects we may assume S_s is constant, the source terms in equation 6 are irrelevant. Therefore, we may use the standard Valet-Fert spin diffusion equation to solve the bulk spin accumulation leading to the general expression for the spin dependent potentials in the bulk:

$$\mu_{\uparrow,\downarrow}(x) = A + Bx \pm C/\sigma_{\uparrow,\downarrow}e^{-x/\lambda_i} \pm D/\sigma_{\uparrow,\downarrow}e^{x/\lambda_i} \quad (7)$$

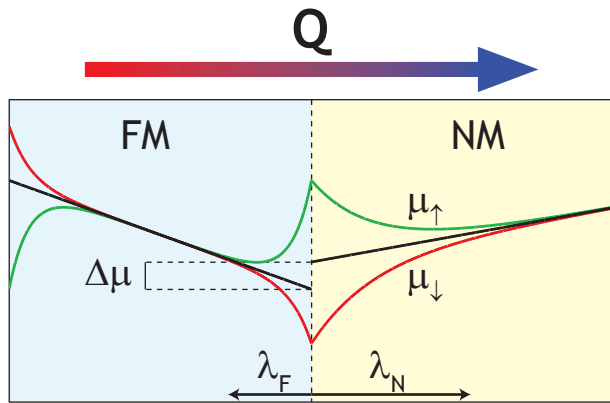


FIG. 6: **Thermal spin injection by the spin Seebeck coefficient across a FM/NM interface.** Schematic figure showing the resulting spin dependent chemical potentials $\mu_{\uparrow,\downarrow}$ across a FM/NM interface when a heat current $Q = -k\nabla T$ crosses it. Heat current is taken to be continuous across the interface leading to a discontinuity in ∇T . No currents are allowed to leave the FM, nevertheless, a spin current proportional to the spin Seebeck coefficient flows through the bulk FM which needs to become unpolarized in the bulk NM. This injects a spin imbalance $\mu_{\uparrow} - \mu_{\downarrow}$ at the boundary which relaxes in the FM and NM with the length scale of their respective spin relaxation lengths λ_i . A thermoelectric interface potential $\Delta\mu = P\mu_s$ also builds up^{1,2}. On the left side no spin current is allowed to leave leading to an opposite spin accumulation.

with A-D the parameters to be solved in both regions. At the FM/NM interface we take the chemical potentials $\mu_{\uparrow,\downarrow}$ to be continuous as well as the spin dependent currents $J_{\uparrow,\downarrow}$. At the outer interfaces we set the spin dependent currents to zero. This leads to a set of equation which can be solved. We obtain:

$$B = e \frac{\sigma_{\uparrow}S_{\uparrow} + \sigma_{\downarrow}S_{\downarrow}}{\sigma_{\uparrow} + \sigma_{\downarrow}} \nabla T_{FM} \equiv eS_{FM}\nabla T_{FM} \quad (8)$$

where we use the definition of the conventional Seebeck coefficient of a ferromagnet S_{FM} ³. The spin accumulation at the interface is:

$$\frac{\mu_s}{\nabla T_{FM}} = e\lambda_F S_s R_{mis} \quad (9)$$

where $R_{mis} = R_N/(R_N + R_F/(1 - P^2))$ is a conductivity mismatch⁴ factor in which $R_i = \lambda_i/\sigma_i$ are the spin resistances determined by the relaxation lengths λ_i and the conductivities σ_i .

IV. SUPPLEMENTARY INFORMATION B

A SEM picture of the previous sample is shown in figure 7 (a). A regular spin valve signal was measured by sending a current from contact 1 to 3 and measuring the potential between contact 5 and 4 of which the result is shown in figure 7 (b). In this case a 13.8 mΩ background

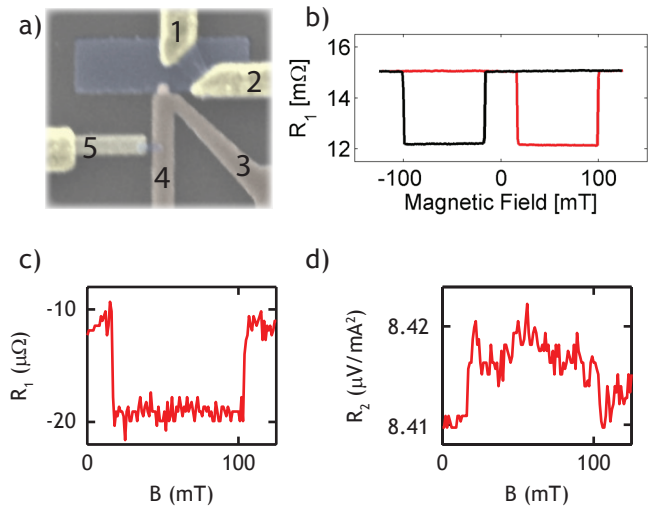


FIG. 7: **Previous device results.** a) Coloured SEM figure of the device. The sample consist of the same two ferromagnets which are now placed 400 nm apart. It is connected by a copper V shape instead of a funnel. b) Non local spin valve signal by sending current from contact 1 to 3 and measuring the potential from contact 5 to 4. c,d) Thermal spin injection result. The current is now send from contact 1 to 2 while the potential was measured between contacts 5 and 4.

R_1^b is observed on top of a non local spin valve signal R_1^s of 3 m Ω . The background is originating from Peltier heating/cooling of the FM/NM interfaces⁵. Both signals are close to the calculated 14.1 m Ω and 4.1 m Ω .

When the current is send from contact 1 to 2, we obtain the results shown in figure 7 (c,d). A regular spin valve signal R_1^s of 10 $\mu\Omega$ is observed on top of a small -15 $\mu\Omega$ background R_1^b . This is somewhat different then the calculated -100 $\mu\Omega$ background and -4 $\mu\Omega$. However, these effects are highly dependent on the exact geometry and are due to the small 30 x 30 nm² size of the contact. This makes sure grain size, lithographic precision and ballistic effects dominate.

Thermal spin injection was observed and is shown in figure 7 (d). The background R_2^b is again larger then the calculated 3.4 $\mu V/mA^2$. If we compensate for this in the modelling we obtain from the observed ≈ -7 nV/mA²

signal a spin Seebeck coefficient for Permalloy of ≈ -5 $\mu V/K$.

We note that our thermal spin injection signals $R_2^s I^2$ cannot be due to an induced temperature dependence of $R_1^s I$ because $R_3^s I^3$, representing the Joule heating induced change of $R_1^s I$ should be ≈ 10 times larger then the possible Peltier heating induced $R_2^s I^2$ at the currents we used in both samples. However, $R_3^s I^3$ was simultaneously measured and found absent. Furthermore, The signal $R_1^s I$ of both devices is of different sign, excluding any further dependence of $R_2^s I^2$ on $R_1^s I$.

We conclude that also in this device we have good agreement between observed and calculated thermoelectric voltages when we apply a similar correction for the Joule heating. A very similar value for the spin Seebeck coefficient was found.

* Electronic address: A.Slachter@rug.nl

¹ van Son, P.C., van Kempen, H. & Wyder, P. Boundary Resistance of the Ferromagnetic-Nonferromagnetic Metal Interface. *Phys. Rev. Lett.* **58**, 2271-2273 (1987)

² Valet, T. & Fert, A. Theory of the perpendicular magnetoresistance in magnetic multilayers. *Phys. Rev. B.* **48**, 7099-7113 (1993)

³ Barnard R.D. Thermoelectricity in metals and alloys. (Taylor and Francis LTD., London, 1972)

⁴ Schmidt, G., Ferrand, D., Molenkamp, L.W., Filip, A.T. & van Wees, B.J. Fundamental obstacle for electrical spin injection from a ferromagnetic metal into a diffusive semiconductor. *Phys. Rev. B* **62**, R4790 (2000)

⁵ Bakker, F.I., Slachter, A., Adam, J.D.M. & van Wees, B.J. Interplay of Peltier and Seebeck effects in nanoscale nonlocal spin valves, submitted to PRL